JGR Biogeosciences

RESEARCH ARTICLE
10.1029/2020JG005678

Key Points:
- The first study to identify optimum temperatures for photosynthetic production in subtropical coastal ecosystems is presented
- The optimum temperature range for photosynthesis of 24.1°C to 27.4°C is often exceeded under the current climate
- Predicted future global warming will result in rapid decline net ecosystem exchange in Australian subtropical coastal ecosystems

Correspondence to:
H. A. McGowan,
h.mcgowan@uq.edu.au

Citation:
McGowan, H. A., Lowry, A. L., & Gray, M. A. (2020). Identification of optimum temperatures for photosynthetic production in subtropical coastal ecosystems: Implications for CO_2 sequestration in a warming world. *Journal of Geophysical Research: Biogeosciences*, *125*, e2020JG005678. https://doi.org/10.1029/2020JG005678

Received 5 FEB 2020
Accepted 28 JUL 2020

Author Contributions:
Formal analysis: Andrew L. Lowry, Michael A. Gray
Investigation: Michael A. Gray
Methodology: Andrew L. Lowry, Michael A. Gray
Project administration: Michael A. Gray
Resources: Michael A. Gray
Validation: Andrew L. Lowry
Visualization: Andrew L. Lowry
Writing - original draft: Andrew L. Lowry, Michael A. Gray
Writing – review & editing: Andrew L. Lowry, Michael A. Gray

©2020. American Geophysical Union. All Rights Reserved.

Identification of Optimum Temperatures for Photosynthetic Production in Subtropical Coastal Ecosystems: Implications for CO_2 Sequestration in a Warming World

Hamish A. McGowan[1], Andrew L. Lowry[1], and Michael A. Gray[1,2]

[1]Atmospheric Observations Research Group, The University of Queensland, Brisbane, Queensland, Australia, [2]Bureau of Meteorology, Brisbane, Queensland, Australia

Abstract Terrestrial ecosystems are often thought to be effective sinks of anthropogenic CO_2 emissions with biosphere greening considered unequivocal evidence of this process. Increasing atmospheric concentrations of CO_2 along with other greenhouse gases are however, responsible for global warming. As temperature increases, the rate at which biomes sequester CO_2 may decline as the optimum temperature for photosynthetic production is exceeded, thereby reducing their potential to sequester CO_2. Here we present evidence from 3 years of direct measurements of CO_2 exchanges over subtropical coastal ecosystems in eastern Australia that the optimum temperature range for photosynthesis of 24.1°C to 27.4°C is routinely exceeded. This causes a rapid decline in photosynthetic production made worse when soil water content decreases. As climate change continues, both rising temperatures and predicted decline in rainfall will see these coastal ecosystems ability to sequester CO_2 decrease further rapidly. We suggest similar research is needed urgently over other terrestrial ecosystems.

Plain Language Summary Emissions of CO_2, primarily from the combustion of fossil fuels, have long been considered to result in an enhanced greening of terrestrial ecosystems through CO_2 fertilization. However, increases in atmospheric CO_2 along with other greenhouse gases have caused global warming. As air temperatures increase, the optimum temperature at which ecosystems sequester CO_2 from the atmosphere may be exceeded and CO_2 uptake by ecosystems declines. This results in more CO_2 including from anthropogenic emissions remaining in the atmosphere where it may cause further warming and climate change. Here we present the first direct measurements of CO_2 exchange over three subtropical coastal ecosystems in Australia. We find that the optimum temperature range for photosynthetic production (CO_2 sequestration from the atmosphere) of 24.1°C to 27.4°C is often exceeded and that predicted future warming will result in a rapid decline in the ability of the coastal ecosystems to sequester CO_2.

1. Introduction

CO_2 fertilization of terrestrial ecosystems in response to anthropogenic CO_2 emissions has been linked to increased net ecosystem production (*NEP*) and associated greening of terrestrial biomes (Los, 2013; Zhang et al., 2019; Zhu et al., 2016). However, *ceteris paribus* CO_2 sequestration in ecosystems, primarily by plants, is temperature dependent. Accordingly, as global temperatures continue to increase, possibly outpacing the evolutionary capability for plants to respond physiologically, the effectiveness of terrestrial ecosystems to act as net sinks of anthropogenic CO_2 emissions will eventually decline. Resulting feedbacks may further accelerate global warming and changes in weather and climate including frequent extremes, such as drought that may place additional stress on critical terrestrial sinks of atmospheric CO_2. The majority of research on plant photosynthesis response to increasing temperatures has focused to date on leaf-scale measurements and identification of optimum leaf temperature for photosynthesis (Hughes, 2000; Way & Yamori, 2014). While these observations have been upscaled in global ecosystem models, they do not account for real world ecosystem complexity, which may result in ecosystem-scale optimum temperatures for photosynthetic production being markedly different from optimum leaf temperatures for photosynthesis (Field et al., 1995; Huang et al., 2019). Urgency is therefore required to develop understanding of ecosystems responses to temperature and the corresponding ability to sequester atmospheric CO_2.

The rare studies conducted to date that have investigated optimum temperatures (T_{opt}) for photosynthetic production indicate that these threshold temperatures may be close, or exceeded, in some regions. At the Large-scale Biosphere-Atmosphere tropical forest site in Brazil, Doughty and Goulden (2008) found that the tropical forest was near its maximum temperature threshold above which CO_2 sequestration decreased sharply. Observed threshold ambient air temperatures for tropical plants range from 26°C to 34°C (Ishida et al., 1999; Keller & Lerdau, 1999; Lerdau & Throop, 1999; Mooney & Koch, 1994). Ma et al. (2017) analyzed 15 years (2000–2015) of eddy covariance (EC) data from flux towers in a Californian oak grass savannah and found the entire ecosystem T_{opt} to be 19.2 ± 0.5°C. This value could vary more than 10°C in response to changes in light intensity, air dryness, and soil moisture thereby highlighting the importance of weather and climate variability in ecosystem CO_2 fluxes. In the high latitudes of the Northern Hemisphere, evidence is also emerging of recent declines in CO_2 uptake, possibly linked to warming (Piao et al., 2017). Peñuelas et al. (2017) found that at 47 sites covering all major types of forest biomes that tree growth rate had not responded significantly over the past 40 years to increased atmospheric CO_2 fertilization. They concluded that other factors, such as increase in temperature, must be coming into play to counter the expected increase in tree biomass.

The subtropics cover the area from latitude 23.5° to 35° north and south. The dominant atmospheric circulation of this climate zone is the subtropical ridge formed by the descending limb of the Hadley cell circulation (Cherchi et al., 2018). Resulting local meteorology is characterized in general by extended periods of settled anticyclonic weather, which is responsible for the subtropical deserts. Distinct wet seasons occur where the ridges interact with monsoons, high-latitude baroclinic systems or they direct maritime air masses onshore. The subtropics in the Southern Hemisphere has expanded poleward by around 2° to 3° over the past 40 years (Cai et al., 2012; Hu & Fu, 2007; Seidel et al., 2008) with evidence making a strong link to global warming and stratospheric ozone depletion (Southern Hemisphere) as the primary forcing mechanisms of this movement.

To date, no observational study has investigated the T_{opt} for photosynthetic production in subtropical ecosystems. Fernández-Martínez et al. (2019), however, used the multidecadal inversion models MACC-II (Monitoring Atmospheric Composition and Climate-Interim Implementation) and the Jena CarboScope and DGVMs (TRENDY) to investigate the global impact of rising CO_2 concentrations on *NEP* relative to change in precipitation, temperature and deposition of nitrogen and sulfur. Results showed that rising CO_2 concentrations were primarily responsible for increased *NEP* but that increasing temperature from 1995–2014 had diminished uptake of CO_2 by terrestrial ecosystems (Fernández-Martínez et al., 2019). The coarse spatial scales and large uncertainties associated with such global modeling necessitates direct measurement of CO_2 exchange over ecosystems, including the subtropics, to accurately quantify the links between rising temperatures and CO_2 atmosphere-ecosystem exchange.

Here we present analysis of EC measurements of CO_2 exchange and associated micrometeorology over three coastal ecosystems in subtropical eastern Australia. We calculate the optimum temperature for photosynthetic production for each ecosystem and show that this value is now being exceeded and likely to result in substantial decreases in CO_2 uptake. The most rapid decline in CO_2 sequestration with increasing temperature above T_{opt} is found to occur over wetland and swamp ecosystems, while a slower decline is seen over a pine plantation. We highlight the urgency for similar research to enable more accurate prediction of future carbon budgets as global temperatures continue to rise.

2. Physical Setting

Research was conducted in the subtropical east coast of Australia where a series of large sand barrier islands fringe Moreton Bay, Queensland, Australia. The northernmost of these, Bribie Island, covers approximately 149 km^2 and has a coastal fringe and a central swale covered by remnant native vegetation, while the central area of the island contains an established commercial pine plantation (Armstrong & Cox, 2002) (Figure 1). The topography is of low relief with much of Bribie Island only 1–3 m above sea level (asl) (Geoscience Australia, 2015). The EC systems were deployed within the three major vegetation types on Bribie Island (Figure 1). One EC system was installed in *Melaleuca quinquenervia* dominated palustrine wetland (referred to as the Wetland site, 26.959°S, 153.144°E, 2.5 m asl). The tree height ranged from 5 to 14 m; the understory was primarily thick fern and sedges (Queensland Herbarium, 2013) with an average basal area of

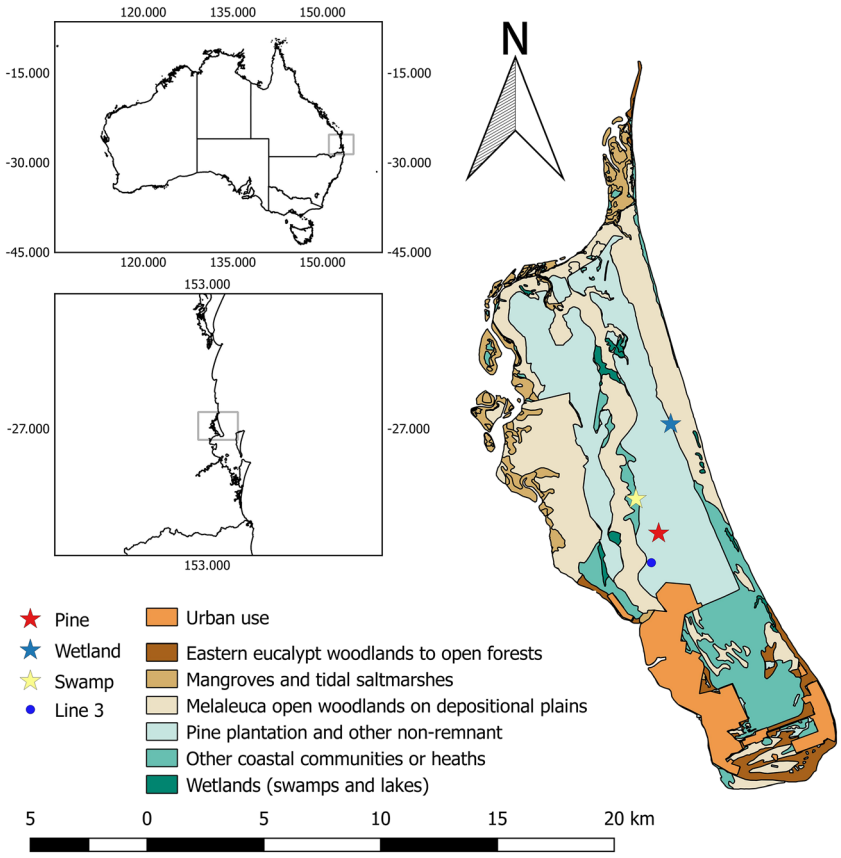

Figure 1. Map of Bribie Island showing the three EC sites (stars), Line 3 rain gauge (blue circle), and the surface cover throughout the island.

32.4 m^2 ha^{-1} and average stem density of 588 stems ha^{-1} (Ryan, 2012). A second EC system was located in a seasonally waterlogged central swale (the Swamp site, 26.988°S, 153.130°E, 2.5 m asl). Vegetation consisted of closed sedge land and heath (Queensland Herbarium, 2013) up to 1.2 m tall. A third EC system was installed in the island's commercial pine plantation (the Pine site, 27.001°S, 153.139°E, 9 m asl), covering approximately 30.9 km^2 and primarily a Honduran Caribbean Pine-Slash Pine hybrid (*Pinus elliottii var. elliottii x Pinus caribaea var. hondurensis*) with an understory of the *Xanthorrhoea* species. Plantation density was 840 trees ha^{-1} and basal area 29.1 m^2 ha^{-1} (Fan et al., 2014). The pine trees at this site were generally 10–15 m tall and were 10–11 years old at the commencement of the research.

Bribie Island lies in a subtropical climate zone with most rainfall events occurring between October and March (Wilson et al., 2013). Mean annual rainfall is approximately 1,411 mm yr^{-1}, while temperature records from Brisbane Airport, 50 km south, suggest approximate minimum and maximum temperatures of 20°C and 30°C in summer and 10°C and 20°C in winter (Bureau of Meteorology, 2019a, 2019b). Throughout the year the predominant winds are on-shore sea breezes and southeasterly trade winds, although during winter dry southeasterly and southwesterly winds are common as cold fronts travel over southern Australia (Tessendorf et al., 2010).

Analysis of a 100 year (1919–2018) air temperature record from the Bureau of Meteorology's Moreton Island station (# 040043) located around 30 km east of Bribie Island with a very similar maritime aspect shows that the mean air temperature of the decade (2008–2018) was +0.74°C warmer than for the first decade (1919–1929) of the record. This warming has been most pronounced since 1990 at a rate of +0.29°C per decade, reflecting the widely acknowledged global warming trends linked to anthropogenic greenhouse gas loading of the atmosphere.

Table 1
Eddy Covariance Site Instrumentation

Instrument and manufacturer	Variables measured	Measurement accuracy
CSAT3 3-D sonic anemometer; Campbell Scientific, USA.	3-D wind components (*ux*,*uy*,*uz*); wind speed and direction; sonic temperature	*ux*, *uy*: < ±8 cm s^{-1}; *uz*: < ±4 cm s^{-1}
81,000 3-D sonic anemometer; RM Young, USA.	3-D wind components (*ux*,*uy*,*uz*); wind speed and direction; sonic temperature	±5 cm s^{-1}
EC150 infrared gas analyzer; Campbell Scientific, USA.	H_2O and CO_2 gas densities	2%
CNR4 net radiometer; Kipp & Zonen, The Netherlands.	Incoming/outgoing shortwave and longwave radiation	Uncertainty in daily total: Pyranometer: <5%, Pyrgeometer: <10%
Pro v2 U23-002; HOBO, USA.	Temperature, relative humidity	±0.21°C, ±2.5%
100K6AIA; BetaTherm, Ireland.	Ambient temperature	±0.15°C
CS650; Campbell Scientific, USA.	Volumetric water content (SWC); soil temperature	SWC: ±3%; ±0.5°C
LI-190SB Quantum sensor; LICOR, USA.	Photosynthetically active radiation (PAR)	<1%
PTB110; Vaisala, Finland.	Barometric pressure (kPa)	±0.15 kPa

Observations presented here were made from late 2012 to late 2015: the Wetland site from 27 June 2013 to 31 Marc 2015, the Pine site from 27 November 2012 to 17 March 2015, and the Swamp site from 27 November 2012 to 1 December 2015 (Gray et al., 2018). The Swamp site was impacted by a wildfire on 9 January 2013 with a resulting loss of all foliage and nonwoody vegetation, followed by a period of regrowth.

3. Methods

3.1. Instrumentation

EC systems and meteorological sensors (Table 1) were secured to a boom on top of pneumatic telescopic masts at the Wetland and Pine sites at heights of 15.5 and 17 m, respectively, and on a 2.4-m tripod at the Swamp site. Each EC system consisted of a Campbell Scientific EC150 infrared gas analyzer (IRGA) and CSAT3 sonic anemometer. Raw 10-Hz data were logged, along with 30-min time-averaged fluxes of CO_2 and latent and sensible heat. Slow response sensor measurements of atmospheric pressure, ambient and soil temperature, soil water content (SWC), and incoming and outgoing shortwave and longwave radiation were logged at 30-min intervals. Each radiometer was positioned a minimum of 2 m outward from the mast or tripod to minimize the influence of the structures on the sensor fields of view. A photosynthetically active radiation (PAR) sensor was installed at the Swamp site on 20 October 2015. Rainfall measurements were obtained from existing rain gauges (1-mm tipping bucket) (Figure 1) (Gray et al., 2018).

SWC sensors were installed on 23 October (Swamp), 20 September (Pine), and 23 September 2013 (Wetland) and remained until the end of observations. At the Pine and Wetland sites the period of operation included two wet seasons and one dry season, with the first wet season receiving below average rainfall (−400 mm compared to the 1961–1990 mean; Bureau of Meteorology, 2019b) and the second wet season receiving above average rainfall (+100 mm compared to 1961–1990 mean; Bureau of Meteorology, 2019b). For each of the three sites the SWC data were split into three, illustrating conditions under dry, moderate, and high levels of soil moisture. The volume of SWC that demarcated each third of the data varied between sites due to differences in substrate type. For example, the Pine site is situated on a sandy elevated surface and an entire third of the SWC data was measured at 0 m^3 m^{-3}; conversely at the Swamp site the driest third of the SWC data was ≤0.295 m^3 m^{-3}. At the Swamp site there was a significant period of inundation after 24 January 2015, which has been assigned to an additional fourth SWC class.

The Wetland site CSAT3 failed in late-August 2014 and was replaced by an RM Young 81,000 3-D sonic anemometer (RMY) on 16 September 2014. A comparison between the CSAT3 and RM Young 81,000 over grass showed excellent agreement for wind speed and direction, and good agreement for sensible heat flux (RMY = 0.95·CSAT3 + 1.46, R^2 = 0.99, RMSE = 5.62. Units are W m^{-2}). The Pine site CSAT3 failed on 9 April 2014, and following repairs, the site was operational again on 16 July 2014.

3.2. Data Analysis

3.2.1. Data Processing and Corrections

High-frequency EC data were processed using a custom software package CRGFlux (Gray et al., 2018). The half-hourly EC data were rotated using the planar fit coordinate rotation method of Wilczak et al. (2001). The data were despiked using a three-step process. First, unreasonable values were removed by visual inspection; then data were removed due to low IRGA signal strength (<0.7) and during periods of rainfall; lastly a 6-point moving average filter was calculated over three iterations to remove data >3 standard deviations from the mean. A simple linear interpolation was applied to fill gaps of up to 90 min (30 min during sunrise or sunset). Transfer functions to correct frequency response due to sensor separation, low-pass filtering, and path length averaging were applied using the methods of Massman (2000) and Massman and Clement (2005). Density effects were corrected in the turbulent fluxes (Webb et al., 1980). The CO_2 flux was corrected for storage effects using the CO_2 concentration at measurement height described by Pilegaard et al. (2001).

The roughness length (z_0) and displacement height (d) were estimated for the Pine and Wetland sites using the method of Martano (2000). For the Swamp site, due to high uncertainty, estimates of d were calculated using the 2/3 h rule (Oke, 1987) and z_0 was estimated using field observations and values from Oke (1987), Stull (1988), and Wieringa (1993).

3.2.2. Carbon Flux Processing

The flux footprint was calculated using the Horst and Weil (1992) model and the summary provided in Horst and Weil (1994). Surface area maps were examined to determine the maximum allowable fetch in a given direction and data where the 90% isopleth exceeded the vegetation of interest in the up or cross wind directions were removed.

Issues with the underestimation of EC measurements at night are well known. To mitigate these effects, friction velocity (u_*) filtering is applied using the method of Reichstein et al., (2005). Data were split into six temperature classes and within each temperature class 20 u_* classes. The u_* threshold is determined where the u_* at lower classes reaches 95% of the average of the higher classes. Thresholds are only kept where there is a weak correlation ($|r| < 0.4$) between temperature and u_*. The final u_* threshold is then determined as the median of the temperature classes thresholds. Following the above processing steps, there was 63% of data remaining at the Wetland, 67% at the Pine, and 46% at the Swamp. This is a common issue with EC data and complete time series data sets were established through robust gap filling (Falge et al., 2001) procedures.

3.2.3. CO_2 Gap Filling

The first step in the gap filling procedure was to fill the meteorological variables that drive the nonlinear regressions (air temperature, solar radiation, and vapor pressure deficit, *VPD*). In the first instance, data were linearly interpolated between the other EC sites. In each case, the site with the highest correlation (R^2) was used first followed by the other site. Typical values of R^2 ranged between 0.89–0.99 for temperature and solar radiation and 0.66–0.74 for *VPD*. For the remaining gaps in the data, temperature and *VPD* were filled from two nearby Bureau of Meteorology weather stations at Beerburrum (Station # 040284) and Redcliffe (Station # 040958) located approximately 15 km west and 26 km southwest of the field area, respectively. The solar radiation data were filled using ERA-Interim data (Isaac et al., 2017; Vuichard & Papale, 2015). The linear interpolation between the ERA-Interim data and EC towers was forced to a zero intercept to prevent negative values of radiation ($R^2 = 0.89$).

With a complete time series of meteorological data, gaps in the CO_2 flux record were filled. The time series was separated into seasons (cool/dry and warm/wet) running from May–October and November–April, based on the absolute humidity threshold of 12 g m^{-3}. To fill nocturnal gaps, the respiration equation of Lloyd and Taylor (1994) is estimated from

$$F_{CO_2} = R_{ref} e^{\left[E_0\left(\frac{1}{T_{ref} - T_0} - \frac{1}{T - T_0}\right)\right]} \quad (1)$$

where T is the temperature in K, T_0 is 227.13 K, T_{ref} is the reference temperature in a given season, and R_{ref} is the CO_2 respiration at the reference temperature. T_{ref} varied from 15–20°C at the Pine and Wetland and 15–25°C at the Swamp. It was necessary to allow T_{ref} to vary between seasons due to a small diurnal variation within each season and marked difference between warmer (November–April) and cooler (May–

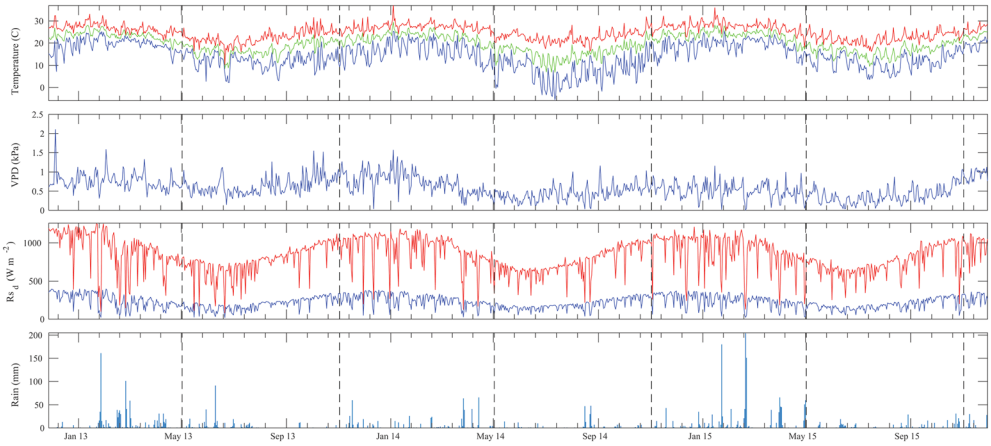

Figure 2. Meteorological conditions from the Swamp site (first panel) daily minimum temperature (blue), average temperature (green), and maximum temperature (red); (second panel) daily average vapor pressure deficit; (third panel) daily average (blue) and maximum (red) incoming shortwave radiation; and (fourth panel) daily rainfall from the nearby rain gauge.

October) seasons (see Figure 2). Temperature sensitivity (E_0) (Reichstein et al., 2005) was then estimated using least squares nonlinear regression for the whole season from the nocturnal u_* filtered time series. R_{ref} was estimated using Levenberg-Marquardt least squares nonlinear regression over 15-day windows with a 10-day overlap from nocturnal measurements. A minimum of six data points were required to perform the nonlinear regression (Reichstein et al., 2005).

Daytime net ecosystem exchange (*NEE*) was calculated from (Lasslop et al., 2010):

$$NEE = \frac{\alpha\beta R_d}{\alpha R_d + \beta} + \gamma \tag{2}$$

where γ is Equation 1, R_d is incoming shortwave solar radiation, α is the initial slope of the light response curve, and β is the photosynthetic capacity at light saturation (Lasslop et al., 2010). β is defined as a decreasing exponential function at high *VPD*.

$$\beta = \begin{cases} \beta_0 \exp(-k(VPD - VPD_0)), & VPD > VPD_0 \\ \beta_0, & VPD \leq VPD_0 \end{cases} \tag{3}$$

where VPD_0 is 10 hPa (Lasslop et al., 2010). Equation 2 was estimated from daytime u_* filtered data using Levenberg-Marquardt least squares nonlinear regression over 15-day windows using E_0 and an initial estimate for R_{ref} from nocturnal measurements. The nonlinear regression was sensitive to the initial estimate for β. To resolve this, we changed the initial value for β to half and double the initial value (Lasslop et al., 2010). The final value for β corresponds to the lowest RMSE from the nonlinear regression. The bounds for the parameters $E_0, R_{ref}, \alpha, \beta$, and k are taken from Lasslop et al., (2010) and gaps in the parameters R_{ref}, α, β, and k are linearly interpolated.

3.2.4. Optimum Temperature for Photosynthesis

As the EC footprint extends over many thousands of square meters, thereby measuring ecosystem-scale processes, we use the "big leaf" analogy of Tan et al. (2017). For consistency with Tan et al. (2017), daytime *NEE* is regarded as equivalent to net photosynthesis rate (P_n) at the leaf level. The optimum temperature for photosynthesis (T_{opt}) can be determined from the temperature response of light-saturated photosynthesis (Tan et al., 2017). To calculate T_{opt} we first filtered the data for the light saturation point from the nonrectangular hyperbolic fit of Equation 2. The light saturation point was determined for each site and season following a visual inspection of light saturation curves for our three sites. We then fitted a peak function to the *NEE* at light saturation to obtain net ecosystem photosynthesis rate under light saturation (μmol m^{-2} s^{-1}) (NEE_{sat}) as a function of air temperature (T_K) as proposed by Tan et al., (2017):

Table 2
Calibrated Parameterizations of Fitted Coefficients b, c, NEE_{25} and T_{max} (Equation 4) With Upper/Lower 95% Confidence Limits Shown in Brackets

Site	b	c	NEE_{25} (μmol m^{-2} s^{-1})	T_{max} (K)
Wetland	11,978 ± 3,647 (8,330, 15,626)	0.874 ± 0.444 (0.429, 1.318)	15.26 ± 0.24 (15.02, 15.50)	305.8 ± 1.5 (304.4, 307.3)
Swamp	25,807 ± 14,390 (11,416, 40,197)	0.328 ± 0.174 (0.154, 0.502)	7.86 ± 0.95 (6.92, 8.81)	308.1 ± 1.3 (306.8, 309.4)
Pine	56,362 ± 83,833 (−27,472, 140,196)	0.12 ± 0.077 (0.043, 0.197)	29.47 ± 62.49 (−33.02, 91.96)	303.6 ± 22.7 (280.9, 326.3)

$$NEE_{sat} = \frac{NEE_{25}\exp\left(\frac{b(T_K - 298)}{298RT_K}\right)}{[1 + \exp(c(T_K - T_{max}))]^2} \quad (4)$$

where R is the universal gas constant. We used light-saturated air temperature at the ecosystem level as a proxy for leaf temperature found in leaf level studies (Tan et al., 2017). To provide an initial estimate of the coefficients in Equation 4, NEE_{25} was taken from the mean NEE_{sat} ($T = 25 \pm 0.2$°C), and T_{max} was estimated at 35°C in line with the locally observed maximum temperatures. The remaining coefficients of b and c were initially estimated at 10,000 and 0.5 respectively. Following fitting of the peak function, the values of b and c were refined for each ecosystem as shown in Table 2 with the 95% confidence limits.

3.2.5. Leaf Area Index

The leaf area index (LAI) was calculated from Moderate Resolution Imaging Spectroradiometer (MODIS) satellite imagery, using the LAI product described in Paget and King (2008). The Swamp site was calculated from a single pixel and the Wetland and Pine sites were the average of 2 and 4 adjacent pixels, respectively, surrounding the EC sites. All pixels used were entirely representative of the vegetation associated with each site. The time series was then created by first linearly interpolating any missing pixels and then applying a 32-day (five observations, 8 days apart) moving average filter centered on the observation date.

4. Results

4.1. Meteorology

The background meteorological conditions from the Swamp site are presented in Figure 2 and highlight the general seasonal conditions across the three measurement sites. The time series was broken down into distinct wet and dry seasons based on a mean monthly absolute humidity threshold of 12 g m^{-3} (Mamadou et al., 2014). The wet season ran from 1 November to 30 April, shown as the vertical dashed lines in Figure 2. There is an obvious seasonality to the temperatures experienced on Bribie Island, with the wet season mean daily temperature ~6°C warmer than the dry season. The dry season in 2014 was noticeably cooler than the other seasons due to much lower nocturnal temperatures. The mean wet season maximum temperature was 26.6°C for the Wetland and Pine sites, and 27.0°C for the Swamp site.

The mean daily *VPD* was slightly lower (0–0.2 kPa) at the Swamp site compared to the Wetland site, and 0.2–0.4 kPa lower than the Pine site. The same water availability relationship was found for the SWC with the Swamp site having 0.2 m^3 m^{-3} more than the Wetland and 0.4 m^3 m^{-3} more than the Pine site. The SWC at the Pine site was consistently <0.15 m^3 m^{-3}, and a third of the SWC data was 0 m^3 m^{-3}. All sites achieved soil saturation following heavy rainfall in January 2015.

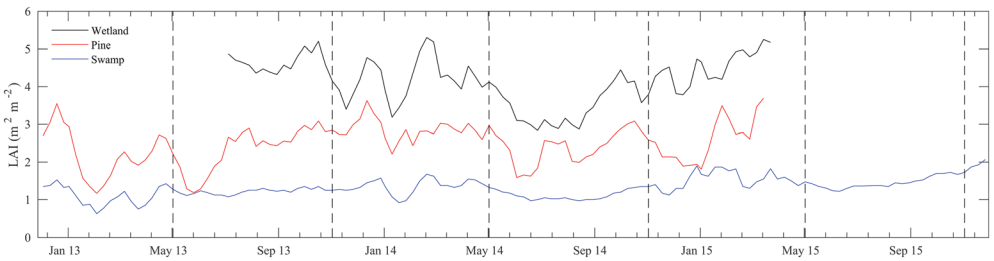

Figure 3. Leaf area index for the three sites from MODIS satellite imagery using a 5-data point moving average filter.

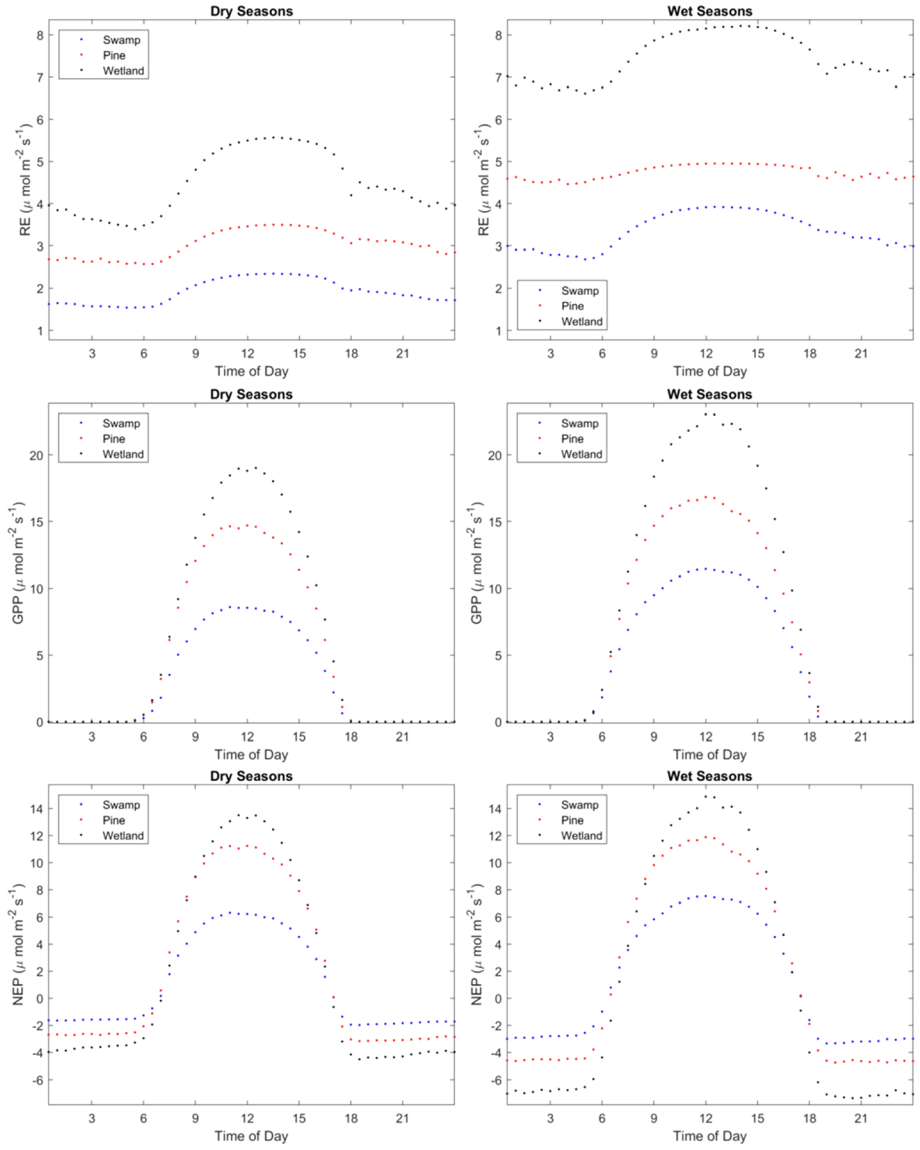

Figure 4. Daily ecosystem respiration (top), gross primary production (middle), and net ecosystem production (bottom) for the dry (left) and wet (right) seasons for each of the three EC sites (Figure 2).

The incoming maximum solar radiation ranged from 1,100 W m^{-2} in summertime to 700 W m^{-2} in winter in cloud free conditions. Incoming solar radiation exceeded 600 W m^{-2} on 90% of wet season days and 83% of dry season days. The rainfall on Bribie Island showed a distinct seasonality between wet and dry seasons, with notable heavy rainfall events (>100 mm day^{-1}) occurring on 27 November 2013, 25 February 2013, 20–21 February 2015, and 23 January 2015. These events led to the inundation of the Swamp site from 27 January until 1 September 2013 and again from 20 February 2015 until the end of observations. The 2012/2013 and 2014/2015 wet seasons received above average rainfall (+200 mm; Bureau of Meteorology, 2019b), and the 2013/2014 was below average (−400 mm; Bureau of Meteorology, 2019b). The three dry seasons received below average rainfall: 2013, −100 mm; 2014, −200 mm; and 2015, −100 mm (Bureau of Meteorology, 2019b).

The LAI for the three EC sites is shown in Figure 3. The LAI at the Pine site is comparable to that found by Fan et al. (2014, 2015), who measured the LAI using a LAI-2000 plant canopy analyzer up to October 2013. The LAI at the Swamp site declines following the fire in January 2013 and then slowly recovers for the remainder of the observation period. There is an underlying seasonality to the Pine and Wetland LAI,

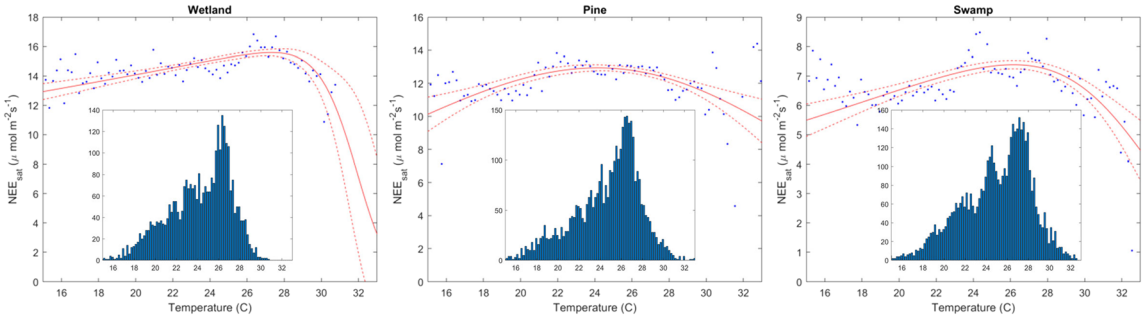

Figure 5. NEE_{sat} (μmol m^{-2} s^{-1}) at light saturation versus air temperature (°C) for the three study sites using Equation 4. Blue dots show the 0.2°C bin average for NEE_{sat}. Red curves show the optimal curve fit, weighted by the probability density function of the 0.2°C bin averages, with 95% confidence limits in dashed lines from Table 2. Histogram counts of the 0.2°C temperature bins for each site are embedded within.

although periods of growth and decline are not limited to distinct growing and contracting seasons. The LAI at the Pine site responds positively to rainfall totals of > 50 mm day^{-1}, a response that also exists to a lesser extent at the Wetland site.

The daily patterns of ecosystem exchanges are shown in Figure 4. The Wetland site is the most productive in both the dry and wet seasons compared to the Pine and Swamp, which correlates with the LAI shown in Figure 3. All sites showed an increase in daytime *NEP* in the wet seasons compared to the dry seasons; 0.64, 1.21, and 1.37 μmol m^{-2} s^{-1} at the Pine, Swamp, and Wetland sites respectively. The Wetland site showed the greatest variation between wet and dry season maximum gross primary production (*GPP*) of 4.01 μmol m^{-2} s^{-1}, with smaller variations between the Swamp (2.85 μmol m^{-2} s^{-1}) and the Pine (2.13 μmol m^{-2} s^{-1}) sites. Similarly, the variation between wet and dry season maximum respiration (*RE*) was greatest at the Wetland with 2.64 μmol m^{-2} s^{-1}, compared to the Swamp (1.58 μmol m^{-2} s^{-1}) and Pine (1.46 μmol m^{-2} s^{-1}) sites.

The daytime peak in *GPP* occurred over the 30-min period to 12 noon at all three sites; however, the peak ecosystem respiration was between 12:00 to 14:00 hr in the wet seasons and 13:30 hr in the dry seasons. Ecosystem respiration remained high in the afternoon, particularly at the Pine and Swamp sites in both the wet and dry seasons. The Wetland site also showed a thermally induced increase in respiration during the afternoon, but it returned to nocturnal values after sunset, whereas the Pine and Swamp sites took longer over the twilight hours to return to nocturnal values. This suggests that the Wetland site can respond better to prolonged periods of increased afternoon temperatures, possibly due to the more diverse nature of the ecosystem and diversity in the structural characteristics of the flora. The Pine site showed virtually no diurnal variation in ecosystem respiration in the wet seasons.

4.2. NEE_{sat} Versus Air Temperature

The temperature dependence of NEE_{sat} is shown in Figure 5. The T_{opt} at which NEE_{sat} peaks is between 24.1°C and 27.4°C for the three sites on Bribie Island. All three sites show a similar pattern of relatively constant increase in NEE_{sat} until the optimal temperature. At the Wetland and Swamp sites there is a noticeable reduction in NEE_{sat} after the T_{opt} is reached. At the Pine site the drop off in NEE_{sat} after the T_{opt} is much less pronounced; however, the T_{opt} is much lower than the Swamp and Wetland sites. As temperatures approach and begin to exceed 30°C there is a more pronounced decline in NEE_{sat}. For example, as temperatures increase 1°C above the mean maximum wet season daily temperature (see Figure 2) from the site observations there is a 0.03% (Wetland), 4.0% (Pine), and 2.7% (Swamp) drop in NEE_{sat} from $NEE_{sat}(T_{opt})$. If temperatures rose 4°C above current observations, as may be the case in scenario Representative Concentration Pathway (RCP) 8.5 by 2090 (CSIRO and Bureau of Meteorology, 2015), then there is a 19.3% (Wetland), 13.8% (Pine), and 20.3% (Swamp) decline in NEE_{sat} below $NEE_{sat}(T_{opt})$. When temperatures exceeded T_{opt} this resulted in lost NEE_{sat} of 3,400 μmol m^{-2} s^{-1} at the Wetland, 6,971 μmol m^{-2} s^{-1} at the Pine and 14,512 μmol m^{-2} s^{-1} at the Swamp below the thermally optimal $NEE_{sat}(T_{opt})$. From the 2–3 years of data at each site, the maximum daily temperature exceeded T_{opt} on 90 days (14.0%) at the Wetland, 497 days (59.2%) at the Pine, and 423 days (38.5%) at the Swamp.

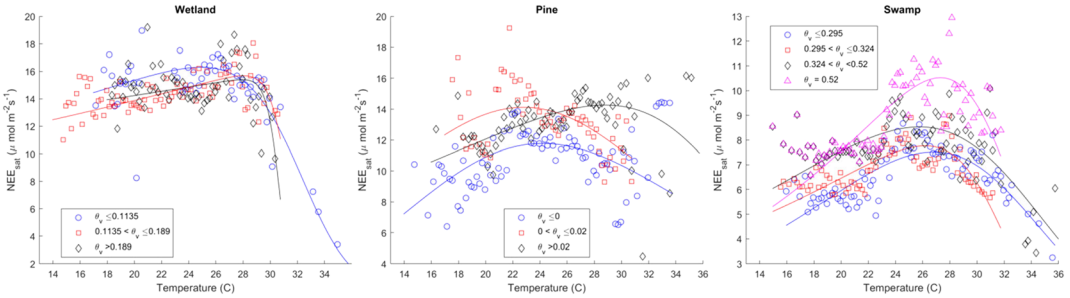

Figure 6. NEE_{sat} as a function of air temperature (°C) separated by SWC (θ_v) for the Wetland (left), Pine (middle), and Swamp (right) sites.

4.3. T_{opt} Affected by SWC

Figure 6 shows that when SWC is limited (the lowest class for each site) there is a reduction in NEE_{sat} above T_{opt}. At the middle SWC class this trend is still evident but there are fewer data at higher temperatures above T_{opt}. For the higher SWC class there is still a drop in NEE_{sat} above T_{opt} at all three sites. At the Wetland and Pine sites there are fewer data points for temperatures >30°C, so some caution is required when considering these results. Nonetheless, results show that as SWC decreases NEE_{sat} decreases above T_{opt}, suggesting that if rainfall decreases as temperatures continue to increase as predicted (CSIRO and Bureau of Meteorology, 2015), then this will accelerate the decline in NEE_{sat}. This is supported by observations from the Swamp site, where there are many more data points above 30°C, including for the period of inundation, although during this period the maximum temperature was 31.75°C. This site showed a marked decline in NEE_{sat} under all noninundated SWC conditions as temperatures increased above 30°C.

5. Discussion

The three ecosystems investigated demonstrated different responses to variations in air temperature. The optimum temperature at which each ecosystem maximized CO_2 uptake was highest at the natural, unmodified Wetland site, slightly lower at the less densely vegetated Swamp site, and lowest at the modified monoculture of the commercial Pine site. The Wetland site consists of many different plant species, greater vegetation density and has a well-established root structure, compared to the other two sites. These factors give the Wetland site greater capacity to respond to extremes in temperature and water stress. Contrastingly at the Pine site, where the 10 to 15-year-old trees are in their growth phase, the NEE_{sat} of this ecosystem was lower than the Wetland site. In particular, when temperatures rise above 24.1°C, NEE_{sat} declines at the Pine site, which occurred on 59% of the days in the observation period. When water does become available at the Pine site, in the form of higher SWC, the NEE_{sat} at this site increases under light saturating conditions. However, our results clearly show that in this coastal subtropical location, replacing native ecosystems with commercial pine plantations, particularly in areas susceptible to lower SWC, lowers the region's ability to sequester CO_2. Furthermore, as temperatures continue to rise, commercial pine plantations on Bribie Island would seem far less capable to respond to the warming temperatures than natural ecosystems.

Our findings of a decrease in NEE_{sat} across all three study sites agrees with the findings of Fernández-Martínez et al. (2019), who found that at a global scale increasing temperatures between 1995 and 2014 had a negative effect on the *NEE*. In tropical climates, Tan et al. (2017) found T_{opt} to be between 23.7°C and 28.1°C but that if water is not limited then the optimum temperature for ecosystem photosynthesis may be as high as 30°C. However, as air temperatures rise above this value, whole of canopy tropical forest CO_2 uptake has been observed to decline by 35% to 40% (Doughty & Goulden, 2008). While future warming will cause rainfall in some tropical regions to increase, in the subtropics and Mediterranean climate zones it is likely to decrease (Spinoni et al., 2018). Sperlich et al. (2019) found reduced rainfall and drought to lower T_{opt} by 22% to 29% in four Mediterranean climax tree species leading to reduced growth and increased risk of tree mortality. Collectively, such research highlights the importance of understanding the impacts of both increasing temperatures and water stress on acclimation of photosynthesis. Our results are similar to Tan

et al. (2017) and importantly extend such research into the subtropics, a region where observations of optimum temperature for photosynthesis are rare (Huang et al., 2019).

In eastern Australia temperatures are expected to rise by 1°C by 2030 under RCP 4.5 relative to 1986–2005 levels and 4°C by 2090 under RCP 8.5 (CSIRO and Bureau of Meteorology, 2015). These increases in temperature will also be accompanied by a decrease in precipitation and higher evaporation rates (CSIRO and Bureau of Meteorology, 2015)—a trend already evident in meteorological records for the past 50 years. Increases in temperatures, above the thermally optimal level at which plants can assimilate CO_2, are controlled by stomatal processes. As temperatures increase, plant atmospheric water availability decreases, thus reducing stomatal conductance (Tan et al., 2017). There is therefore an indirect relationship between temperature and stomatal processes and its corresponding effects on optimum temperature. In our findings, increases in temperature above the thermal optimum corresponded with decreases in NEE_{sat} as water availability decreases. The consequences for the Bribie Island ecosystems for a warming and drying climate are likely to be significant decreases in net ecosystem photosynthesis.

6. Conclusion

As global temperatures continue to rise and precipitation becomes more variable, understanding how CO_2 exchange between the surface and the atmosphere may change over different ecosystems is critical to predictions of future atmospheric CO_2 concentrations and impacts on climate. Here we have shown for the first time in a subtropical setting, the optimum temperatures for NEE_{sat} over two common natural ecosystems (Swamp and Wetland) and a monoculture commercial pine plantation are between 24.1°C to 27.4°C. When temperatures exceed these values, NEE_{sat} decreases rapidly, a response that is made worse when SWC decreases.

Under the current climatic conditions (late 2012 to late 2015) the maximum daily temperature already exceeded T_{opt} on 14.0% of days at the Wetland and 59.2% and 38.5% of days at the Pine and Swamp sites respectively. This resulted in a reduction of NEE_{sat} of 6,971 μmol m^{-2} s^{-1} at the Pine site compared to 3,400 μmol m^{-2} s^{-1} at the Wetland site. Accordingly, under current conditions (2012–2015) the *Melaleuca quinquenervia*-dominated palustrine Wetland site is least affected by periods when T_{opt} is exceeded, highlighting its high value in CO_2 sequestration compared to its replacement by commercial Pine plantations. However, as temperatures increase this ecosystem will likely experience the most rapid decrease in NEE_{sat}, followed by the Swamp, then Pine. Collectively, this will result in a corresponding decrease in CO_2 sequestration from the atmosphere, which will accelerate as temperatures continue to warm and exceed T_{opt} for longer periods. This will positively feedback into the climate system and contribute to increasing the rate of global warming. We plan to extend this research to other climate zones and their ecosystems in Australia.

Data Availability Statement

The data used in this study has been published and can be accessed online (at https://doi.org/10.14264/uql.2019.687).

Acknowledgments
The authors thank Queensland Parks and Wildlife Service and HQ Plantations for allowing site access and all field assistants. This study was sponsored by The National Centre for Groundwater Research and Training (NCGRT), cofunded by the Australian Research Council and the National Water Commission. M. Gray received funding from an Australian Government Research Training Program Scholarship and from the School of Earth and Environmental Sciences at The University of Queensland.

References

Armstrong, T. J., & Cox, M. E. (2002). The relationship between groundwater and surface water character and wetland habitats, Bribie Island, Queensland. In A. Haig, D. George, & S. Tickell (Eds.), *Balancing the groundwater budget, Proceedings of the 7th IAH National Groundwater Conference*. Northern Territory, Australia: Darwin.

Bureau of Meteorology (2019a). Australian Water Availability Project Rainfall data http://www.bom.gov.au/jsp/awap/rain/index.jsp

Bureau of Meteorology (2019b). Climate Data Online http://www.bom.gov.au/climate/data/

Cai, W., Cowan, T., & Thatcher, M. (2012). Rainfall reductions over Southern Hemisphere semi-arid regions: The role of sub-tropical dry zone expansion. *Scientific Reports*, *2*(1), 702. https://doi.org/10.1038/srep00702

Cherchi, A., Ambrizzi, T., Behera, S., Carolina, A., Freitas, V., Morioka, Y., & Zhou, T. (2018). The response of subtropical highs to climate change. *Current Climate Change Reports*, *4*(4), 371–382. https://doi.org/10.1007/s40641-018-0114-1

CSIRO and Bureau of Meteorology (2015). Climate change in Australia Information for Australia's Natural Resource Management Regions: Technical Report, CSIRO and Bureau of Meteorology, Australia.

Doughty, C. E., & Goulden, M. L. (2008). Are tropical forests near a high temperature threshold? *Journal of Geophysical Research*, *113*, G00B07. https://doi.org/10.1029/2007JG000632

Falge, E., Baldocchi, D., Olson, R., Anthoni, P., Aubinet, M., Bernhofer, C., et al. (2001). Gap filling strategies for defensible annual sums of net ecosystem exchange. *Agricultural and Forest Meteorology*, *107*(1), 43–69. https://doi.org/10.1016/S0168-1923(00)00225-2

Fan, J., Oestergaard, K. T., Guyot, A., Jensen, D. G., & Lockington, D. A. (2015). Spatial variability of throughfall and stemflow in an exotic pine plantation of subtropical coastal Australia. *Hydrological Processes*, *29*(5), 793–804. https://doi.org/10.1002/hyp.10193

Fan, J., Oestergaard, K. T., Guyot, A., & Lockington, D. A. (2014). Measuring and modeling rainfall interception losses by a native Banksia woodland and an exotic pine plantation in subtropical coastal Australia. *Journal of Hydrology*, *515*, 156–165. https://doi.org/10.1016/j.jhydrol.2014.04.066

Fernández-Martínez, M., Sardans, J., Chevallier, F., Ciais, P., Obersteiner, M., Vicca, S., et al. (2019). Global trends in carbon sinks and their relationships with CO_2 and temperature. *Nature Climate Change*, *9*(1), 73–79. https://doi.org/10.1038/s41558-018-0367-7

Field, C. B., Randerson, J. T., & Malmström, C. M. (1995). Global net primary production: Combining ecology and remote sensing. *Remote Sensing of Environment*, *51*(1), 74–88. https://doi.org/10.1016/0034-4257(94)00066-V

Geoscience Australia, (2015). In: Commonwealth of Australia Canberra (Ed.), digital elevation model (DEM) of Australia derived from LiDAR 5 metre grid, https://doi.org/10.4225/25/5652419862E23

Gray, M., McGowan, H., Lowry, A., & Guyot, A. (2018). Surface energy exchanges over contrasting vegetation types on a sub-tropical sand island. *Agricultural and Forest Meteorology*, *249*, 81–99. https://doi.org/10.1016/j.agrformet.2017.11.018

Horst, T. W., & Weil, J. C. (1992). Footprint estimation for scalar flux measurements in the atmospheric surface layer. *Boundary-Layer Meteorology*, *59*(3), 279–296. https://doi.org/10.1007/BF00119817

Horst, T. W., & Weil, J. C. (1994). How far is far enough?: The fetch requirements for micrometeorological measurement of surface fluxes. *Journal of Atmospheric and Oceanic Technology*, *11*(4), 1018–1025. https://doi.org/10.1175/1520-0426(1994)011<1018:HFIFET>2.0.CO;2

Hu, Y., & Fu, Q. (2007). Observed poleward expansion of the Hadley circulation since 1979. *Atmospheric Chemistry and Physics*, *7*(19), 5229–5236. https://doi.org/10.5194/acp-7-5229-2007

Huang, M. T., Piao, S. L., Ciais, P., Peñuelas, P., Wang, X., Keenan, T. F., et al. (2019). Air temperature optima of vegetation productivity across global biomes. *Nature Ecology and Evolution*, *3*(5), 772–779. https://doi.org/10.1038/s41559-019-0838-x

Hughes, L. (2000). Biological consequences of global warming: Is the signal already apparent? *Trends in Ecology & Evolution*, *15*(2), 56–61. https://doi.org/10.1016/S0169-5347(99)01764-4

Isaac, P., Cleverly, J., McHugh, I., van Gorsel, E., Ewenz, C., & Beringer, J. (2017). OzFlux data: Network integration from collection to curation. *Biogeosciences*, *14*(12), 2903–2928. https://doi.org/10.5194/bg-14-2903-2017

Ishida, A., Nakano, T., Matsumoto, Y., Sakoda, M., & Ang, L. (1999). Diurnal changes in leaf gas exchange and chlorophyll fluorescence in tropical tree species with contrasting light requirements. *Ecological Research*, *14*(2), 77–88. https://doi.org/10.1046/j.1440-1703.1999.00291.x

Keller, M., & Lerdau, M. (1999). Isoprene emission from tropical forest canopy leaves. *Global Biogeochemical Cycles*, *13*(1), 19–29. https://doi.org/10.1029/1998GB900007

Lasslop, G., Reichstein, M., Papale, D., Richardson, A. D., Arneth, A., Barr, A., et al. (2010). Separation of net ecosystem exchange into assimilation and respiration using a light response curve approach: Critical issues and global evaluation. *Global Change Biology*, *16*(1), 187–208. https://doi.org/10.1111/j.1365-2486.2009.02041.x

Lerdau, M. T., & Throop, H. L. (1999). Isoprene emission and photosynthesis in a tropical forest canopy: Implications for model development. *Ecological Applications*, *9*(4), 1109–1117. https://doi.org/10.1890/1051-0761(1999)009[1109:IEAPIA]2.0.CO;2

Lloyd, J., & Taylor, J. A. (1994). On the temperature dependence of soil respiration. *Functional Ecology*, *8*(3), 315–323. https://doi.org/10.2307/2389824

Los, S. O. (2013). Analysis of trends in fused AVHRR and MODIS NDVI data for 1982–2006: Indication for a CO_2 fertilization effect in global vegetation. *Global Biogeochemical Cycles*, *27*, 318–330. https://doi.org/10.1002/gbc.20027

Ma, S., Osuna, J. L., Verfaillie, J., & Baldocchi, D. D. (2017). Photosynthetic responses to temperature across leaf-canopy-ecosystem scales: A 15-year study in a Californian oak-grass savanna. *Photosynthesis Research*, *132*(3), 277–291. https://doi.org/10.1007/s11120-017-0388-5

Mamadou, O., Cohard, J. M., Galle, S., Awanou, C. N., Diedhiou, A., Kounouhewa, B., & Peugeot, C. (2014). Energy fluxes and surface characteristics over a cultivated area in Benin: Daily and seasonal dynamics. *Hydrology and Earth System Sciences*, *18*(3), 893–914. https://doi.org/10.5194/hess-18-893-2014

Martano, P. (2000). Estimation of surface roughness length and displacement height from single-level sonic anemometer data. *Journal of Applied Meteorology*, *39*(5), 708–715. https://doi.org/10.1175/1520-0450(2000)039<0708:EOSRLA>2.0.CO;2

Massman, W., & Clement, R. (2005). Uncertainty in eddy covariance flux estimates resulting from spectral attenuation. In X. Lee, W. Massman, & B. Law (Eds.), *Handbook of micrometeorology: A guide for surface flux measurement and analysis* (pp. 67–99). Netherlands, Dordrecht: Springer. https://doi.org/10.1007/1-4020-2265-4-4

Massman, W. J. (2000). A simple method for estimating frequency response corrections for eddy covariance systems. *Agriculture and Forest Meteorology*, *104*(3), 185–198. https://doi.org/10.1016/S0168-1923(00)00164-7

Mooney, H. A., & Koch, G. W. (1994). The impact of rising CO_2 concentrations on the terrestrial biosphere. *Ambio*, *23*(1), 74–76.

Oke, T. R. (1987). *Boundary layer climates* (2nd ed.p. 435). New York: Methuen.

Paget, M., & King, E. (2008). MODIS land data sets for the Australian region. CSIRO Marine and Atmospheric Research internal report 004, https://doi.org/10.4225/08/585c173339358

Peñuelas, J., Ciais, P., Canadell, J. G., Janssens, I. A., Fernández-Martínez, M., Carnicer, J., et al. (2017). Shifting from a fertilization-dominated to a warming-dominated period. *Nature Ecology and Evolution*, *1*(10), 1438–1445. https://doi.org/10.1038/s41559-017-0274-8

Piao, S., Liu, Z., Wang, T., Peng, S., Ciais, P., Huang, M., et al. (2017). Weakening temperature control on the interannual variations of spring carbon uptake across northern lands. *Nature Climate Change*, *7*(5), 359–363. https://doi.org/10.1038/nclimate3277

Pilegaard, K., Hummelshøj, P., Jensen, N. O., & Chen, Z. (2001). Two years of continuous CO_2 eddy-flux measurements over a Danish beech forest. *Agricultural and Forest Meteorology*, *107*(1), 29–41. https://doi.org/10.1016/S0168-1923(00)00227-6

Queensland Herbarium, (2013). In: Department of Science Information Technology Innovation and the Arts (Ed.), Regional Ecosystem Description Database (REDD). Version 7.1. Department of Environment and Heritage Protection, Brisbane, Australia.

Reichstein, M., Falge, E., Baldocchi, D., Papale, D., Aubinet, M., Berbigier, P., et al. (2005). On the separation of net ecosystem exchange into assimilation and ecosystem respiration: Review and improved algorithm. *Global Change Biology*, *11*(9), 1424–1439. https://doi.org/10.1111/j.1365-2486.2005.001002.x

Ryan, T. S. (2012). *Technical descriptions of regional ecosystems of Southeast Queensland, Queensland Herbarium* (p. 154). Brisbane: Department of Science, Information Technology, Innovation and the Arts.

Seidel, D. J., Fu, Q., Randel, W. J., & Reichler, T. J. (2008). Widening of the tropical belt in a changing climate. *Nature Geoscience*, *1*(1), 21–24. https://doi.org/10.1038/ngeo.2007.38

Sperlich, D., Chang, C. T., Penuelas, J., & Sabate, S. (2019). Responses of photosynthesis and component processes to drought and temperature stress: Are Mediterranean trees fit for climate change? *Tree Physiology*, *39*(11), 1783–1805. https://doi.org/10.1093/treephys/tpz089

Spinoni, J., Vogt, J. V., Naumann, G., Barbosa, P., & Dosio, A. (2018). Will drought events become more frequent and severe in Europe? *International Journal of Climatology*, *38*(4), 1718–1736. https://doi.org/10.1002/joc.5291

Stull, R. B. (1988). *An introduction to boundary layer meteorology* (p. 670). Dordrecht: Kluwer Academic Publishers Group. https://doi.org/10.1007/978-94-009-3027-8

Tan, Z.-H., Zeng, J., Zhang, Y.-J., Slot, M., Gamo, M., Hirano, T., et al. (2017). Optimum air temperature for tropical forest photosynthesis: mechanisms involved and implications for climate warming. *Environmental Research Letters*, *12*(5), 054022. https://doi.org/10.1088/1748-9326/aa6f97

Tessendorf, S. A., Bruintjes, R. T., Weeks, C., Wilson, J. W., Knight, C. A., Roberts, R. D., et al. (2010). Overview of the Queensland cloud seeding research program. *Journal of Weather Modification*, *42*, 89–103.

Vuichard, N., & Papale, D. (2015). Filling the gaps in meteorological continuous data measured at FLUXNET sites with ERA-Interim reanalysis. *Earth System Science Data*, *7*, 157–171.

Way, D. A., & Yamori, W. (2014). Thermal acclimation of photosynthesis: On the importance of adjusting our definitions and accounting for thermal acclimation of respiration. *Photosynthesis Research*, *119*(1-2), 89–100. https://doi.org/10.1007/s11120-013-9873-7

Webb, E. K., Pearman, G. I., & Leuning, R. (1980). Correction of flux measurements for density effects due to heat and water vapour transfer. *Quarterly Journal of the Royal Meteorological Society*, *106*(447), 85–100. https://doi.org/10.1002/qj.49710644707

Wieringa, J. (1993). Representative roughness parameters for homogeneous terrain. *Boundary-Layer Meteorology*, *63*(4), 323–363. https://doi.org/10.1007/BF00705357

Wilczak, J., Oncley, S., & Stage, S. (2001). Sonic anemometer tilt correction algorithms. *Boundary-Layer Meteorology*, *99*(1), 127–150. https://doi.org/10.1023/A:1018966204465

Wilson, L., Manton, M. J., & Siems, S. T. (2013). Relationship between rainfall and weather regimes in south-eastern Queensland. Australia. *International Journal of Climatology*, *33*(4), 979–991. https://doi.org/10.1002/joc.3484

Zhang, Y., Song, C., Band, L. E., & Sun, G. (2019). No proportional increase of terrestrial gross carbon sequestration from the greening Earth. *Journal of Geophysical Research: Biogeosciences*, *124*, 2540–2553. https://doi.org/10.1029/2018JG004917

Zhu, Z., Piao, S., Myneni, R. B., Huang, M., Zeng, Z., Canadell, J. G., et al. (2016). Greening of the Earth and its drivers. *Nature Climate Change*, *6*(8), 791–795. https://doi.org/10.1038/nclimate3004